GNSS-RO Sounding in the Troposphere and Stratosphere

Benjamin Ruston, Neill Bowler, Sean Healy, and Hui Shao

Abstract The use of Global Navigation Satellite System Radio Occultations (GNSS-RO) for vertical sounding of temperature and moisture in the atmospheric column has become a standard practice of many numerical weather prediction (NWP) centers. The introduction of this observation has seen broad positive impact on analyses and forecasts. On longer timescales the impact of the introduction of this data type in re-analyses can be clearly seen. Further, the observations can be used without bias correction and the consistency between sensors is very good allowing these observation to serve as anchoring observations. This is particularly helpful to constrain the bias-correction applied to satellite radiances. In the following chapter we explore the fundamentals of the measurement, the derivation of the typical observation which is used in NWP, the assimilation methods and error assumptions which are used, and finally some conjecture on the direction to improve the use of the observations and what future measurement systems may look like.

B. Ruston (✉)
Naval Research Laboratory (NRL), Monterey, CA, USA
e-mail: ben.ruston@nrlmry.navy.mil

N. Bowler
Met Office, FitzRoy Road, Exeter EX1 3PB, UK
e-mail: neill.bowler@metoffice.gov.uk

S. Healy
European Centre for Medium Range Weather Forecasts (ECMWF), Reading, UK
e-mail: sean.healy@ecmwf.int

H. Shao
Joint Center for Satellite Data Assimilation (JCSDA)/University Corporation for Atmospheric Research (UCAR), College Park, MD, USA
e-mail: huishao@ucar.edu

S. K. Park and L. Xu (eds.), *Data Assimilation for Atmospheric, Oceanic and Hydrologic Applications (Vol. IV)*, https://doi.org/10.1007/978-3-030-77722-7_13

1 Fundamentals of the Radio Occultation Measurement

The concept radio occultation measurements was pioneered in the planetary science community in 1960s and 1970s Kliore et al. (1965), Fjeldbo et al. (1971). The use of radio occultation techniques to measure the Earth's atmosphere was also discussed during that period, but the potential costs appeared prohibitive at the time Yunck et al. (2000). In the 1980s a team at the Jet Propulsion Laboratory (JPL) suggested making radio occultation measurements with the Global Positioning System (GPS). This led to the concept of Global Navigation Satellite Systems radio occultation (GNSS-RO), and the "proof of concept" GPS-MET mission in the mid 1990s Ware et al. (1996). A number research and operational missions followed, including CHAMP Wickert et al. (2001), COSMIC/FORMOSAT-3 Anthes et al. (2008), Metop GRAS Luntama (2008) and, more recently, COSMIC-2/FORMOSAT-7 Schreiner (2020). The earlier missions used the American GPS system, but more recent missions—like COSMIC-2/FORMOSAT-7—are also exploiting other signals such as the Russian GLONASS system.

The GNSS-RO technique at its core is based on the simple physics of refraction. It requires the measurement of a Doppler frequency shift of a transmitted signal by a GNSS receiver Melbourne et al. (1994); Kursinski et al. (1997). The measurement geometry is shown in Fig. 1. The transmitters are typically in a medium earth orbit (with orbital periods around 12 h) and the receivers typically in a low Earth orbit (LEO). The signals propagate from the GNSS satellite to the LEO, but the path is slightly curved as a result of refractive index gradients in both the ionosphere and neutral atmosphere. This curvature or bending of the ray path changes the Doppler shift of the signal, when compared with the Doppler shift that would have been measured for a straight line path between the satellites. Most of the bending occurs over a few hundred kilometers of the ray-path between the satellites, where the signal is closest to the Earth's surface. Because of the availability of precise orbital determination (POD) and stable clocks to high precision, down to femtoseconds, this Doppler shift is well measured and is at the core of the stability of the GNSS-RO observation. The relative motion between the transmitter and receiver provide the sounding through the atmosphere, producing either a rising or setting occultation as it views the transmitter. The transmitted signal is in the microwave spectrum, with commonly used GPS frequencies at $f_1 = 1.57542$ GHz and $f_2 = 1.2276$ GHz, referred to as the GPS L1 and L2 signals. The use of relatively long wavelengths (19.1 cm for L1; 24.4 cm for L2) allows the signals to pass through Earth's atmosphere with little interference from particles such as aerosols or clouds.

A typical occultation sounding of the neutral atmosphere will last about one or two minutes. Due to the satellite motions, a slice of the atmosphere is scanned, and the LEO satellite receives signals where the ray paths have different minimum distances to the surface, from zero up to approximately 100 km. The points where the ray paths have the minimum distance to the surface are commonly referred to as the tangent points. The resulting occultation profile has a relatively higher vertical resolution (about a few hundred meters, varying with heights), compared with other satellite

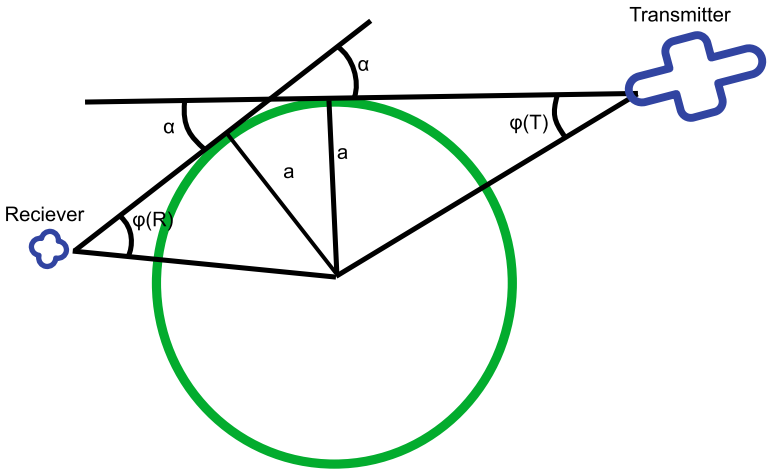

Fig. 1 Schematic of GNSS geometry for a medium Earth orbit transmitter and Low-Earth Orbit (LEO) receiver

measurements. Given the bending measurement reflects the integrated effects along the ray-path in the atmosphere, the horizontal resolution along the ray-path is rather coarse, typically a few hundred kilometers. However, the resolution perpendicular to the "occultation plane" (a plane defined by the positions of a LEO satellite and its occulted GPS satellite, and the center of the local curvature of the occultation) remains fairly high. The measurement from each occultation contains a slanted profile of atmospheric states at each of the tangent points. Due to the satellite motions, the tangent points for one occultation have horizontal shifts, these are as large as 1 degree from the surface to about 40 km (Fig. 2).

The proof of concept GPS-MET mission, led by the Universities Corporation for Atmospheric Research (UCAR), was the first spacebourne sensor to demonstrate the GNSS-RO technique Ware et al. (1996). A series of studies examined data from this early mission and helped to establish the ability of radio occultation to be used for retrievals of temperature Kursinski et al. (1996); Rocken et al. (1997) and geopotential height Leroy (1997) using retrieval techniques developed by planetary scientists. Subsequently information content studies were run, based on variational retieval techniques more closely related to how the measurements would be assimilated into NWP systems. These showed that the GNSS-RO measurements complemented the information provided by high resolution interferometers Collard and Healy (2003), suggesting that these measurements would provide useful information for NWP applications, particularly in the upper troposphere and stratosphere. The key characterisistics that make GNSS-RO measurement an important component of the global observing system are that they can be used without bias correction Eyre (2016), and they have excellent vertical resolution as a result of the limb geometry.

Routine operational assimilation of GNSS-RO measurements into NWP systems began in 2006, and most centres currently assimilate either refractivity

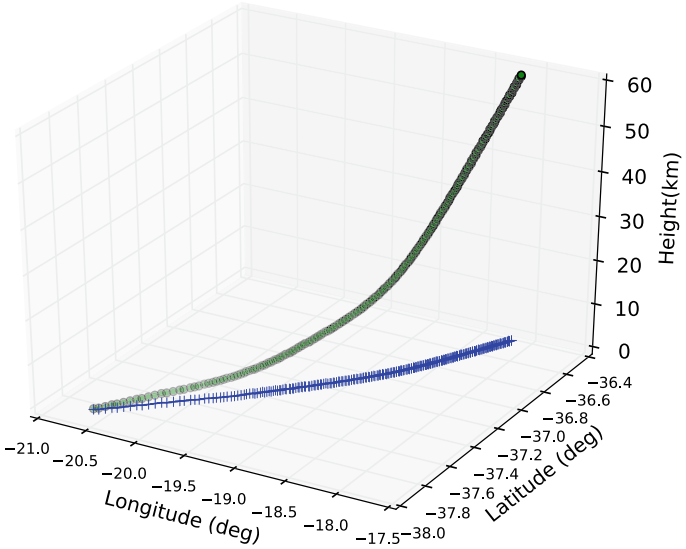

Fig. 2 Tangent point positions (black) as function of impact height (km) and their horizontal projections (blue) within a latitude-longitude plane. The example data are from the COSMIC-2 mission, measured at 11:13 UTC 11 October 2019

or—increasingly—bending angles. The largest impact has generally been seen for upper-tropospheric and stratospheric temperatures, but there are some indications that the latest missions are also having a significant impact lower in the troposphere.

2 Typical Use of GNSS-RO in NWP

2.1 GNSS-RO Processing

It is important to understand the processing of GNSS-RO observations and their information content prior to developing an assimilation strategy. In particular, it should be recognised that GNSS-RO observations are not direct measurements of geophysical quantities such as temperature, pressure and water vapor, even if these quantities can be retrieved from GNSS-RO measurements with a suitable processing system Kursinski et al. (1997), Hajj et al. (2002).

Figure 3 shows a schematic flowchart of the key steps in a GNSS-RO geometrical optics (GO) processing system. The geometrical optics processing assumes that only a single ray arrives at the receiver at a given time, but this is often not the case for ray paths in the troposphere. More than one ray arriving at the receiver is known as "atmospheric multipath". This problem can be mitigated with "wave optics" processing

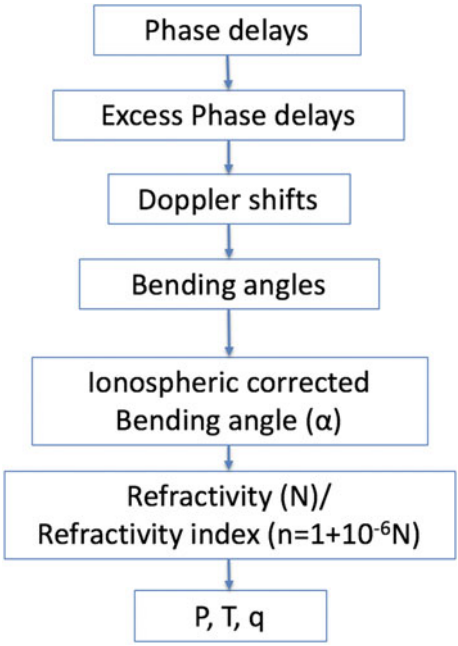

Fig. 3 Schematic flowchart of GNSS-RO measurements and retrievals. P, T and q refer to the air pressure, temperature and specific humidity respectively

techniques, which are essentially a coordinate transforms Gorbunov and Lauritsen (2004); Jensen et al. (2003, 2004) designed to recover the single ray path picture.

Briefly, the GO processing starts with "raw" measurements of the phase delay of radio signals received at two GNSS frequencies during an occultation. Following various calibration and correction procedures Hajj et al. (2002), the "excess" phase delays are computed by subtracting the phase delays expected for a straightline path in a vacuum. The time derivative of the excess phase delays the provide a timeseries of Doppler shift values at both transmitted freqiencies Cucurull et al. (2015).

The total bending angle for each GNSS signal, i, α_i, as a function of the impact parameter, a, can then be derived from the Doppler shift values, by *assuming* that the impact parameter, a, is a constant along the ray-path. This assumption, known as spherical symmetry, implies that horizontal refractive index gradients are zero in the plane of the ray-path, meaning that the refractive index, n, is assumed to be only a function of a height variable, $n(r)$.

The ionospheric contribution to the ray bending can be removed—or corrected—by taking a linear combination of the bending angles at the two GNSS frequencies Vorobev and Krasilnikova (1994). For the the GPS L1 and L2 signals this correction can be writtens as,

$$\alpha(a) = \alpha_1(a) + \frac{f_2^2}{f_1^2 - f_2^2}\left(\alpha_1(a) - \alpha_2(a)\right) \tag{1}$$

where α_1 and α_2 are the bending angles for L1 and L2 signals, interpolated to a common impact parameter value, a, and f_1 and f_2 are the signal frequencies.

The raw observations, of Doppler shift and time delay, are typically measured at high temporal resolution. This corresponds with a very high vertical sampling, much higher than the vertical resolution of NWP models. Therefore, some vertical smoothing is applied to the bending angles and these are sub-sampled to an appropriate resolution in the vertical. This smoothing reduces the noise present in the measurements at the expense of introducing vertical correlations in the errors of the observations. The amount of smoothing applied varies between processing centres, and there is not currently an established procedure for determining the optimal level of smoothing in order to maximise NWP performance.

A key approximation which is often employed to use radio occultation profiles of $\alpha(a)$ is that of spherical symmetry. This assumption can break down, particularly near the surface in the presence of horizontal gradients of humidity. However, making the assumption of spherical symmetry enables the application of an Abel transform pair, relating $\alpha(a)$ to the refractive index, n, as function of a height variable Kursinski et al. (1997). More specifically, the bending angle integral can be written as:

$$\alpha(a) = -2a \int_a^\infty \frac{\frac{d(\ln n)}{dx}}{(x^2 - a^2)^{\frac{1}{2}}} dx \tag{2}$$

where $x = nr$, with r being the radius of a point on the ray path. Conversely, the profile of refractive index is then written as function of $\alpha(a)$,

$$n(x) = \exp\left[\frac{1}{\pi} \int_x^\infty \frac{\alpha(a)}{(a^2 - x^2)^{\frac{1}{2}}} da\right] \tag{3}$$

noting that the upper limit of this integral is ∞, implying some extrapolation of the observed bending angle profile, since it usually stops around 80 km. The extrapolation and smoothing of the bending angles prior to the Abel transform is combined in a processing step known as statistical optimization Healy (2001).

In general, the atmospheric refractive index can be written as function of geophysical quantities via Bean and Dutton (1968); Hajj et al. (2002):

$$N = (n-1)10^6 = a_1 \frac{P}{T} + a_2 \frac{P_w}{T^2} + a_e \frac{n_e}{f^2} + a_w W_w + a_i W_i + O(f^{-3}) \tag{4}$$

where N is known as the refractivity. The quantities on the right hand side are: P_w=$P/(0.622 + 0.378q)$ is the water vapor partial pressure, where P is the air pressure, T is the temperature, q is the specific humidity; n_e is the electron density and f is the signal frequency; W_w and W_i are the liquid water and ice contents; a_1, a_2, a_e, a_w, and a_i are empirical coefficients for each term, respectively. Therefore, refractivity has contributions from four main sources Kursinski et al. (1997), the dry

neutral atmosphere, water vapor, free electrons in the ionosphere and scattering by liquid water and ice particulates.

The ionospheric contribution to N can usually be ignored for NWP applications, because it should be removed with Eq. (1) Vorobev and Krasilnikova (1994). In addition, one can also neglect the scattering by particulates, as for the transmitter frequencies used and for the majority of atmospheric suspensions of water and ice, because their contribution is small compared with other terms in the equation Kursinski et al. (1997); Solheim et al. (1999). This then leaves the dry neutral atmosphere and water vapor terms for the atmosphere typically below about 60 km. This simplifies to an equation using empirically derived constants for a_1 and a_2 Bean and Dutton (1968):

$$N = (n-1)10^6 = 77.6\frac{P}{T} + 3.73 \cdot 10^5 \frac{P_w}{T^2} \tag{5}$$

We note that more sophisticated expressions for refractivity are also used in GNSS-RO data assimilation applications Aparicio and Laroche (2011).

In the stratosphere, and other regions where the contribution of water vapor to the refractivity is small, the refractivity is proportional to density ($N \simeq 77.6\frac{P}{T} \propto \rho$). Given refractivity (or density) as a function of height, the hydrostatic equation can be integrated downwards to give pressure as function of height. The temperature can then be derived by applying the ideal gas law. The temperature retrieved by assuming the humidity can be neglected is often called the "dry temperature" in GNSS-RO.

More generally, when the moisture cannot be neglected – for example in the lower troposphere—the retrieval of T, P and q from N is an under-determined problem and therefore *a priori* information (e.g., an NWP forecast state) is required to solve the geophysical retrieval.

From a data assimilation perspective, the "dry temperature retrievals" outlined here provide a good framework for understanding the measurement technique and understanding assimilation options, but these retrievals are not suitable for direct assimilation into an NWP system.

3 Assimilation Methods and Error Statistic Assumptions

The aim of data assimilation is to combine a forecast of the atmospheric state, $\mathbf{x_b}$, with new observations, $\mathbf{y}$ in a statistically optimal way Lorenc (1986). In variational assimilation methods this involves minimizing a cost function of the form,

$$J(\mathbf{x}) = (\mathbf{x} - \mathbf{x_b})^{\mathbf{T}}\mathbf{B}^{-1}(\mathbf{x} - \mathbf{x_b}) + (\mathbf{y} - H(\mathbf{x}))^{\mathbf{T}}\mathbf{R}^{-1}(\mathbf{y} - H(\mathbf{x})) \tag{6}$$

with respect to $\mathbf{x}$, where $\mathbf{B}$ is the background-error covariance matrix, $\mathbf{R}$ is the observation-error covariance matrix and H is the forward operator, mapping the meteorological state information, $\mathbf{x}$, to observation space. The analysis, $\mathbf{x_a}$, is the

state which minimizes the cost function, and it should be consistent with both $\mathbf{x_b}$ and $\mathbf{y}$, to within their expected error statistics.

Given this general framework, it is clear that the assimilation requires both a good estimate of the GNSS-RO error statistics ($\mathbf{R}$), and an accurate forward operator (H) to map the meteorological state to observation space. These two requirements are not completely independent because the $\mathbf{R}$ matrix is usually assumed to include contributions from both measurements errors, $\mathbf{E}$, and forward model errors, $\mathbf{F}$, so $\mathbf{R} = \mathbf{E} + \mathbf{F}$. The choice of forward model, H, usually represents a trade-off between making $\mathbf{F}$ as small as possible, by including as much physics as possible to retreive all of the available information, versus the computational cost and the timeliness requirements of an operational NWP system.

In addition, it is now generally recognised in NWP that additional processing steps tend to complicate the observation error statistics and correlations. For example, in the context of GNSS-RO, error simulation studies show that vertical error correlations for refractivity tend to be broader than bending angles.

The additional processing steps can also introduce *a priori* information less accurate than the NWP forecast. For example, we do not want to assimilate information provided by a mean state climatology into NWP system. For this reason, it is usually preferable to assimilate variables close to the raw measurement for all observation types. As far as we are aware, no NWP centres assimilate GNSS-RO retrievals of temperature and humidity.

3.1 Forward Operators: H (x)

Eyre (1994) was the first to discuss the GNSS-RO assimilation options in detail. The various processing levels discussed by Eyre are the same as those shown in Fig. 3. At present, most of the operational centres use either the ionospherically-corrected bending angle (Eq. 1) or refractivity (Eq. 3) for data assimilation.

Refractivity Assimilation

When considering assimilation of refractivity, one can use the formulation in Eq (5) as the forward operator to compute the atmospheric refractivity from the model state (T, P, and q) as a function of geopotential height. This is a common approach which was an option taken by many data assimilation systems, e.g., the Gridpoint Statistical Interpolation (GSI) system Cucurull et al. (2007) and the Weather Research and Forecast model Data Assimilation (WRFDA) system. It is relatively straightforward to account for "tangent point drift" in the horizontal plane when assimilating refractivity Cucurull et al. (2007). However, the forward model simulates the refractivity at the horizontal location of the tangent point, while the retrieved refractivity will be related to a quantity which is horizontally averaged in the occultation plane. There are "non-local"(two-dimensional) refractivity and phase operators Syndergaard et al. (2005); Sokolovskiy et al. (2005); Shao et al. (2009) that try account for this by simulating horizontally averaged refractivity values in the two-dimensional occultation plane,

but these are not currently adopted by global operational NWP centres. However, they have been tested in limited-area models Chen et al. (2009).

When considering refractivity assimilation, it is also worth noting the "statistical opimization" step to smooth and extrapolate the bending angles prior performing the Abel transform, Eq.(3). This introduces *a priori* information and for that reason it is advisable not to assimilate the refractivity values above 40 km.

Bending Angle Assimilation

There are several ways to assimilate the GNSS-RO bending angle profiles with varying degrees of complexity. The simplest is a one-dimensional (1D) approach that computes the bending angle integral, Eq (2), at a single representative location Healy (2006), ignoring the actual two-dimensional geometry. Similar to refractivity assimilation, it is straightforward to introduce tangent point drift Poli et al. (2009); Cucurull (2012). The 1D bending angle assimilation technique is an approach broadly adopted by the operational and research communities, given its simplicity and computational efficiency to implement. Rennie (2010) and Cucurull et al. (2013) have both presented experiments comparing such an operator with a refractivity operator in their systems, before switching to the bending angle approach for operational use.

The most complex and accurate GO approach for bending angle assimilation is to simulate bending angle via a ray-tracing method using three-dimensional (3D) refractivity information provided by the NWP forecast. It solves a ray-trajectory equation, which governs the behavior of the radio signal wave under the influence of a refractivity field. The bending angle can be computed by following the ray path. When expressed in a Cartesian coordinate, the general ray-path equation is written as Kravtsov and Orlov (1990):

$$\frac{d^2\mathbf{r}}{ds^2} = n\nabla n \tag{7}$$

where $\mathbf{r}$ is the position vector pointing from the Earth's center to the ray trajectory in the Cartesian coordinate, s is defined by $ds = dl/n$, where l is the length of the ray path and ds is the differential displacement along the ray path. A commonly used form of the ray equation is a set of first-order differential equations:

$$\frac{d\mathbf{r}}{ds} = \mathbf{t} \tag{8}$$

$$\frac{d\mathbf{t}}{ds} = n\nabla n \tag{9}$$

where $\mathbf{t}$ defines the direction of the ray. The ray-trajectory equation can be numerically solved for any given 3D field of n, once either initial conditions (initial position and direction) or boundary conditions (two end point positions) of the ray are prescribed. The boundary problem may require a ray-shooting method, which is expensive computationally and is subject to multiple solutions due to multi-path propagations Zou et al. (1999). Therefore, it is typically solved as an initial value problem. Over the past 20 years, variants of bending angle ray-tracing operators

have been proposed (e.g. Zou et al. (2002); Wee et al. (2010)) but they are not used operationally at the moment.

The 3D ray-tracing method can be simplified by solving the equation in multiple 2D "occultation planes", defined geometrically by the positions of the GNSS and LEO satellites and the local curvature center. Such a bending angle operator is often denoted as a 2D bending angle operator. For a two-dimensional approximation in polar coordinates, ignoring refractive index gradients perpendicular to the GNSS-RO occultation plane, the ray-path equations can be written as Rodgers (2000):

$$\frac{dr}{ds} = cos\phi \tag{10}$$

$$\frac{d\theta}{ds} = \frac{sin\phi}{r} \tag{11}$$

$$\frac{d(\theta + \phi)}{ds} = \frac{-sin\phi}{n}\left(\frac{\partial n}{\partial r}\right)_{\theta} + \frac{cos\phi}{nr}\left(\frac{\partial n}{\partial \theta}\right)_{r} \tag{12}$$

where r and ϕ are the radius and the polar angle at an arbitrary point on the ray path, respectively, θ is the local zenith angle of the ray path.

Implementation of a 2D bending angle operator in an NWP system is more challenging than the 1D operators, since it requires information from multiple horizontal locations of the NWP model state along the specific ray path for each bending angle computation. One such 2D bending angle operator is described by Healy et al. (2007). It is also critical for operational implementation to develop an efficient parallel computing scheme for computational efficiency Healy (2014). Currently, the use of 2D bending angle operators by operational NWP centres is limited Healy (2014). With the advance of computational resources and techniques, 2D or even 3D bending angle assimilation—or other advanced approaches – will be more feasible for operational implementation and research studies.

3.2 Error Statistic Assumptions

As noted above, understanding the measurement errors statistics and using a realistic **R** matrix when assimilating the GNSS-RO measurements is also a key requirement for successfully exploiting these data.

Due to the high precision of the clocks used within the GNSS satellites it is possible for the raw measurements within GNSS-RO to be very precise. Therefore, many of the errors and uncertainties associated with GNSS-RO observations are related to the processing of the measurements and their forward modelling in NWP. These were dealt with in considerable detail in Kursinski et al. (1997) so a brief description will be given here.

At the very highest levels in the neutral atmosphere, the bending induced by the ionosphere can play an important role. The techniques for removing these effects, described above, are not perfect and the residual errors will affect the measured bending angle at upper levels. In the troposphere many of the errors and uncertainties are connected with the variation of water vapour. The calculation of a bending angle from the raw measurement made by the satellite entail an assumption of spherical symmetry (Sect. 2.1). This situation is compounded by many observation operators being one-dimensional which also requires the assumption of spherical symmetry. Although this assumption is reasonable in the stratosphere, it is a poor assumption in the troposphere, since water vapour often varies strongly on short horizontal scales.

These are just two of the main issues which affect GNSS-RO data. Since they affect data at high- and low-levels, GNSS-RO data generally have most impact in the low- to mid-stratosphere. That being said, the observations still play an important role at the other levels.

A commonly used method to estimate the uncertainties in observations is the method of Desroziers et al. (2005). With this method one calculates the cross-product between the innovations and the residuals as

$$E(\mathbf{d}_{\mathrm{o}}^{\mathrm{a}}(\mathbf{d}_{\mathrm{o}}^{\mathrm{b}})^{\mathrm{T}}) = \mathbf{R}_{\mathrm{est}} \tag{13}$$

where $\mathbf{d}_{\mathrm{o}}^{\mathrm{b}}$ is a vector of the differences between the observations and the NWP background forecast (known as the innovations) and $\mathbf{d}_{\mathrm{o}}^{\mathrm{a}}$ is a vector of the differences between the observations and the analysis (known as the residuals). This cross-product provides an estimate of the observation-error covariance matrix. If the data assimilation method used in the analysis is perfect (i.e. is provided with the correct error-covariance matrices and finds the globally optimal solution) then this estimate will correspond to the true observation-error covariance matrix. Thus this method was developed as a consistency check on the inputs provided to the data assimilation. There are other methods to estimate the observation uncertainties Hollingsworth and Lonnberg (1986); Scherllin-Pirscher (2011); Anthes and Rieckh (2018) which may be preferable in certain situations.

Examination of estimated observation uncertainties (the square root of the diagonal elements of $\mathbf{R}_{\mathrm{est}}$) diagnosed using the method of Desroziers indicates that they principally vary with a small number of different quantities Bowler (2020). The key quantities with which the uncertainties vary are the height of the observation, the receiving satellite and the latitude of the tangent point.

The variation of the estimated uncertainty with latitude for Metop-B is shown in Fig. 4. In this (and following figures) the estimated uncertainty has been normalised by the background forecast of the bending angle. This normalisation is chosen because the bending angle can vary by many orders of magnitude with height. In the troposphere the estimated uncertainties are much larger than elsewhere. The reason for this variation is well understood. The tropical troposphere has a high specific humidity. Since water vapour is often not well modelled by NWP systems, in part due to the small-scale variations that it displays, then there are large differences between the observation and the background forecast. In addition the one-dimensional for-

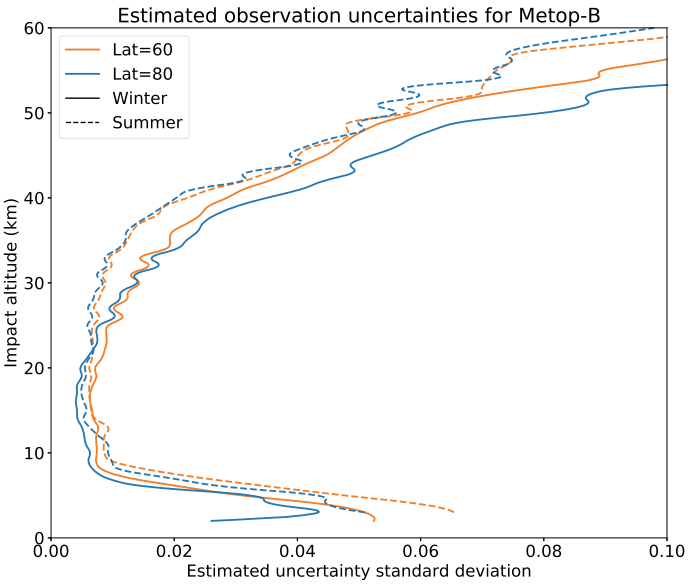

Fig. 4 Diagnosed uncertainties, normalised by the background bending angle, with results binned using a range of latitudes for Metop-B. Each latitude gives the centre of a 20 degree bin, and if the tangent-point of the observation falls within that bin, then the observation is assigned to the given latitude. The statistics for Figs. 4, 5 and 6 are calculated using assimilation statistics from the Met Office's NWP system from the month of January 2020

ward models that are often used (including in the calculation of Fig. 4) make strong assumptions about the spherical symmetry of the atmosphere. These background and forward-modelling errors lead to the observation being ascribed as having large uncertainties.

The variation with receiving satellite is illustrated in Fig. 5. These statistics are calculated from observations within 10 degrees of the equator, so that different latitudinal sampling does not complicate the graph. The statistics from the different satellites are often very similar, despite large differences in the hardware and processing software used. At high altitudes the observation uncertainty estimated for the Metop satellites is much smaller than for the other satellites. This is due to the receiver exhibiting a very low thermal noise and the use of an ultra-stable oscillator in the instrument (C Marquardt, Radio occultation team leader, EUMETSAT, personal communication, 2019).

It is also noticeable that the standard deviation estimated for FY-3C/D is large between around 20–25 altitude. 25km is the height at which the data processing switches from geometric optics to wave optics. For all GNSS-RO data a smoothing is applied to the data within a vertical profile in order to reduce the noise in the data (see Sect. 2.1). The amount of smoothing that is required differs between geometric and wave optics processing. This increase in the standard deviations occurs because the level of smoothing has not been well-matched between the types of processing.

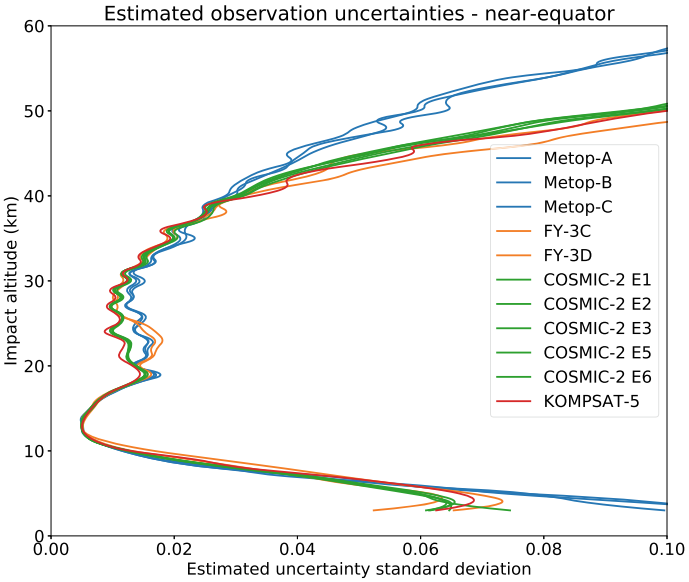

Fig. 5 Diagnosed observation uncertainties, normalised by the background bending angle, with results binned for different satellites. Statistics calculated observations within 10 degrees of the equator

The Metop satellites have the largest standard deviations between around 25–35. This is due to less vertical smoothing being used generally for these satellites.

From the above examples it can be noted that both the hardware used to receive the signals, as well as the software used to process those signals, plays a role in the quality of the observations.

One can also note that the estimated observation uncertainties vary with the season. Figure 6 shows a comparison between the estimated uncertainties in the Northern Hemisphere summer and winter for data from Metop-B. Larger uncertainties are diagnosed in the summer troposphere than in the winter troposphere. This is likely due to the warmer atmosphere containing more water vapour. However, above 25 km altitude the winter atmosphere has larger diagnosed uncertainties. Near the winter pole the average bending angle at high altitudes can become very small. Since the uncertainties are normalised by the background bending angle, this can lead to a larger relative error.

4 GNSS-RO Impact in NWP Systems

In this section we briefly summarise the current impact of GNSS-RO measurements in the ECMWF NWP system. These should be representative of the impact at other NWP centres. The experiments span a 3 month period from January 1 to March

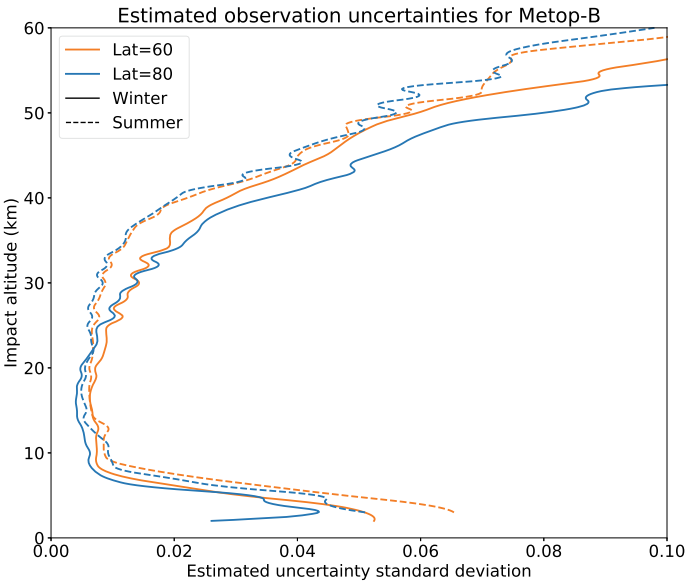

Fig. 6 Diagnosed observation uncertainties, normalised by the background bending angle for Metop-B. Results are shown for different seasons and latitudes in the Northern Hemisphere Extra-Tropics summer (16 June 2018 to 16 July 2018) and winter (January 2020)

31, 2020. They use the ECMWF Integrated Forecast System (IFS) cycle 47R1 in incremental 4D-Var mode, with a 12 h assimilation window. The forecast model is run at Tco399, which is an effective grid spacing of 25 km.

The GNSS-RO data are assimilated with a 2D bending operator. A global bending angle uncertainty model is used, and the assumed uncertainty is only a function of impact height (impact parameter minus radius of curvature). The percentage uncertainty is assumed to fall linearly in impact height from 20 % at 0 km to 1.25 % at 10 km. Above 10 km we assume a constant value of 1.25 % until this reaches a lower limit of 3×10^{-6} rad.

The three experiments shown here are:

1. CONTROL (CTL): Uses the GNSS-RO available operationally at the beginning of 2020, including Metop (A+B+C) GRAS, FY-3C GNOS, TerraSAR-X, Tandem-X and KOMPSAT-5.
2. COSMIC-2 (C2): CTL experiment plus the COSMIC-2 measurements
3. NoRO: CTL minus ALL GNSS-RO measurements

All other observation types used operationally during this period are assimilated in these experiments.

Figure 7 shows the standard deviation of differences between short-range forecasts and globally-distributed radiosonde temperature profiles when the GNSS-RO measurements are assimilated, divided by the standard deviation from the NoRO

experiment. Values less than 100 % indicate that the GNSS-RO are improving the short-range forecasts. The GNSS-RO measurements have a clear positive impact throughout the vertical column, but the largest impact is above 200 hPa, where the percentage improvements exceed 2 % when the COSMIC-2 data are assimilated.

Results qualitatively similar to this have been produced at many NWP centres (e.g., Healy (2006); Cucurull et al. (2007); Aparicio and Deblonde (2008); Rennie (2010)), and they are broadly consistent with earlier GNSS-RO information content studies Collard and Healy (2003), so this is a well established result. In contrast, it has been more difficult to demonstrate a clear impact of GNSS-RO on the humidity fields. However, recent results assimilating COSMIC-2 measurements have now suggested that GNSS-RO are also improving the short-range humidity forecasts. Figure 8 shows the globally averaged short-range forecast departure statistics for ATMS radiances. Channels 6–15 are sensitive to temperature, but channels 18–22 are sensitive to tropospheric humidity. There is a clear improvement in the humidity sensitive channels, of around 1 % when the COSMIC-2 measurements are assimilated. This signal is also reproduced in most other satellite and in situ data types sensitive to tropospheric humidity, and it is an important recent result for GNSS-RO.

Figure 9 shows the combined impact of the GNSS-RO measurements on the medium range forecast error statistics in the COSMIC-2 experiment. This is the fractional change in the zonally averaged standard deviation of the geopotential forecast errors. The forecast errors are calculated using the difference between the forecast and the analysis for each of the experiments (with and without GNSS-RO observations). Values less than 0 (blue) indicate that the forecast errors are being reduced by the GNSS-RO measurements, and hatching indicates statistical significance at the 95 % level. At forecast ranges between T+24h and T+120h there are reductions in the forecast error at most heights and latitudes, demonstrating the broad positive impact of these observations.

5 Future Directions for the Observation and Methods

In the previous sections we outlined some of the general principles applied for use of GNSS-RO in numerical weather prediction in the troposphere and stratosphere. The application described uses transmitters in medium earth orbit and receivers in LEO orbit. However, there are future directions which could expand this network to enhance sampling in areas deemed undersampled, or where it is assumed additional coverage could provide the greatest benefit.

There are two concepts which could help to expand the current GNSS-RO observing network. One of these would be to use a constellation of LEO satellites where one would act as a transmitter and another as a receiver. One such concept uses a wave optics-based retrieval chain Benzon and Hoeg (2016), along with XK and KM bands to probe the atmosphere, allowing for correction of water vapor content, and the potential to explore ozone content Benzon and Hoeg (2016). A network of LEO-LEO satellites could significantly enhance the GNSS-RO network supplying

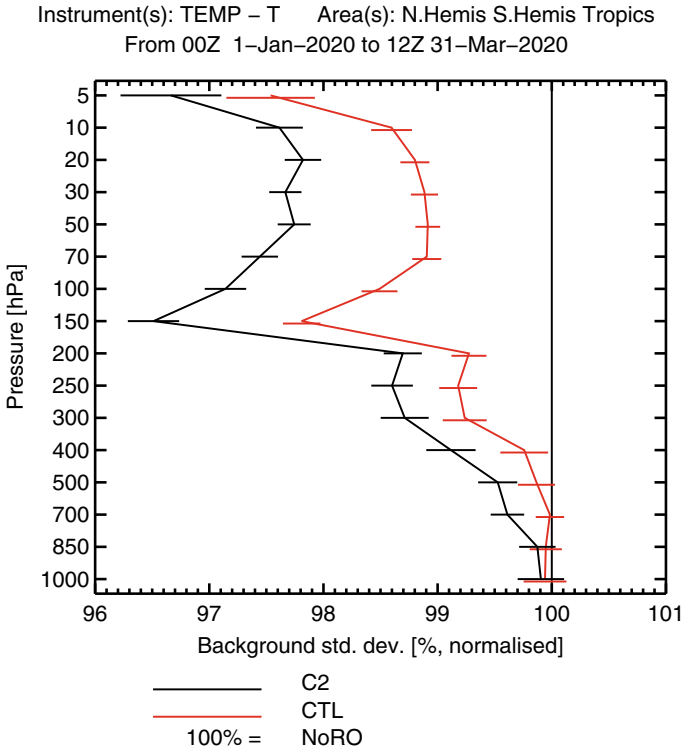

Fig. 7 The normalised standard deviation of short-range forecast departures from radiosonde temperatures on pressure levels, for the C2 (black line) and CTL (red line) experiments. These have been divided by the NoRO standard deviation values, and so values less than 100 % indicate that the GNSS-RO measurements are improving the short-range forecasts

some unique information in addition to current techniques at the L band frequency. A second way to augment the current GNSS-RO network is already being employed which is the implementation on aircraft. This greatly increases the GNSS-RO observation density and has been used for field campaigns. Similar to space-bourne RO, airborne radio occultation (ARO) airborne radio occultation (ARO) measures signal propagation delay from rising and setting GNSS satellites below the local horizon that sample the atmosphere in a region to either side of the aircraft Xie et al. (2008). The application of these ARO could be expanded in the future, a fleet of drones could be deployed to supplement the current GNSS-RO observing network or could be directed for targeted work such as severe weather outbreaks, or extreme weather events.

Another further enhancement of the GNSS-RO observing network could be the use of small and even cube satellites. Since a cube-sat is much cheaper to develop and launch than larger satellites a constellation of cube-sats has the prospect of providing many more observations for a given cost. Various private companies are developing

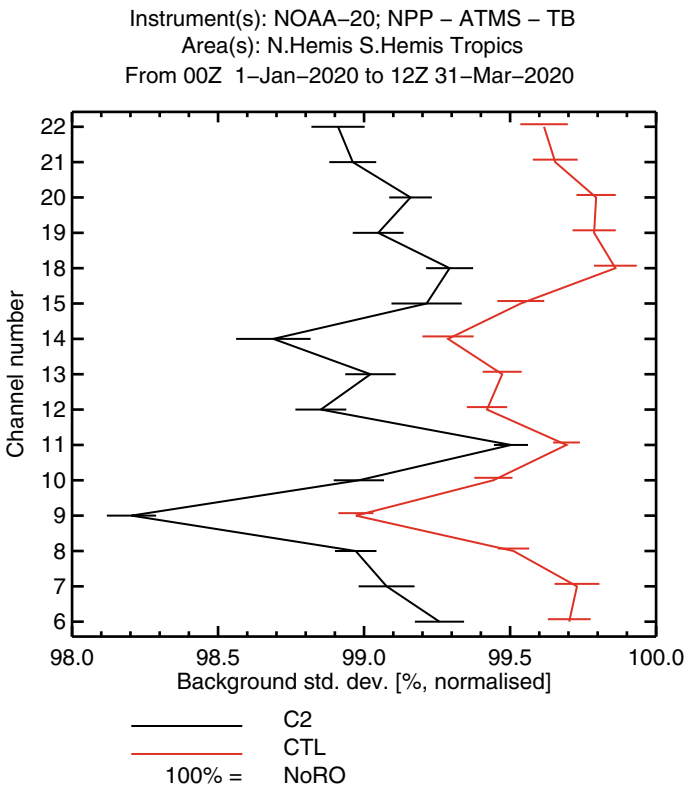

Fig. 8 The normalised standard deviation of short-range forecast departures from ATMS radiances as a function of channel number, for the C2 (black line) and CTL (red line) experiments. These have been divided by the NoRO standard deviation values, and so values less than 100 % indicate that the GNSS-RO measurements are improving the short-range forecasts

such constellations with the hope of selling the observations to government agencies. Preliminary results Bowler (2020); NOAA / NESDIS (2020) indicate that the observations are of sufficient quality for use in NWP. Further, the Met Office and ECMWF assimilated Spire observations operationally in 2020 to help mitigate the loss of aircraft measurements as a result of the COVID-19 pandemic. Figure 10 is the time series of the adjoint based forecast sensitivity to observation impact (FSOI) diagnostic Langland and Baker (2004); Cardinali (2009) in 2020 for the ECMWF operational system. There are two clear jumps in the GNSS-RO (GPSRO) contribution, when COSMIC-2 was assimilated on March 25, 2020 and when Spire data became operational on May 13, 2020. In late March 2020 the contribution from aircraft rapidly decreased as restrictions on air travel greatly reduced the number of observations available.

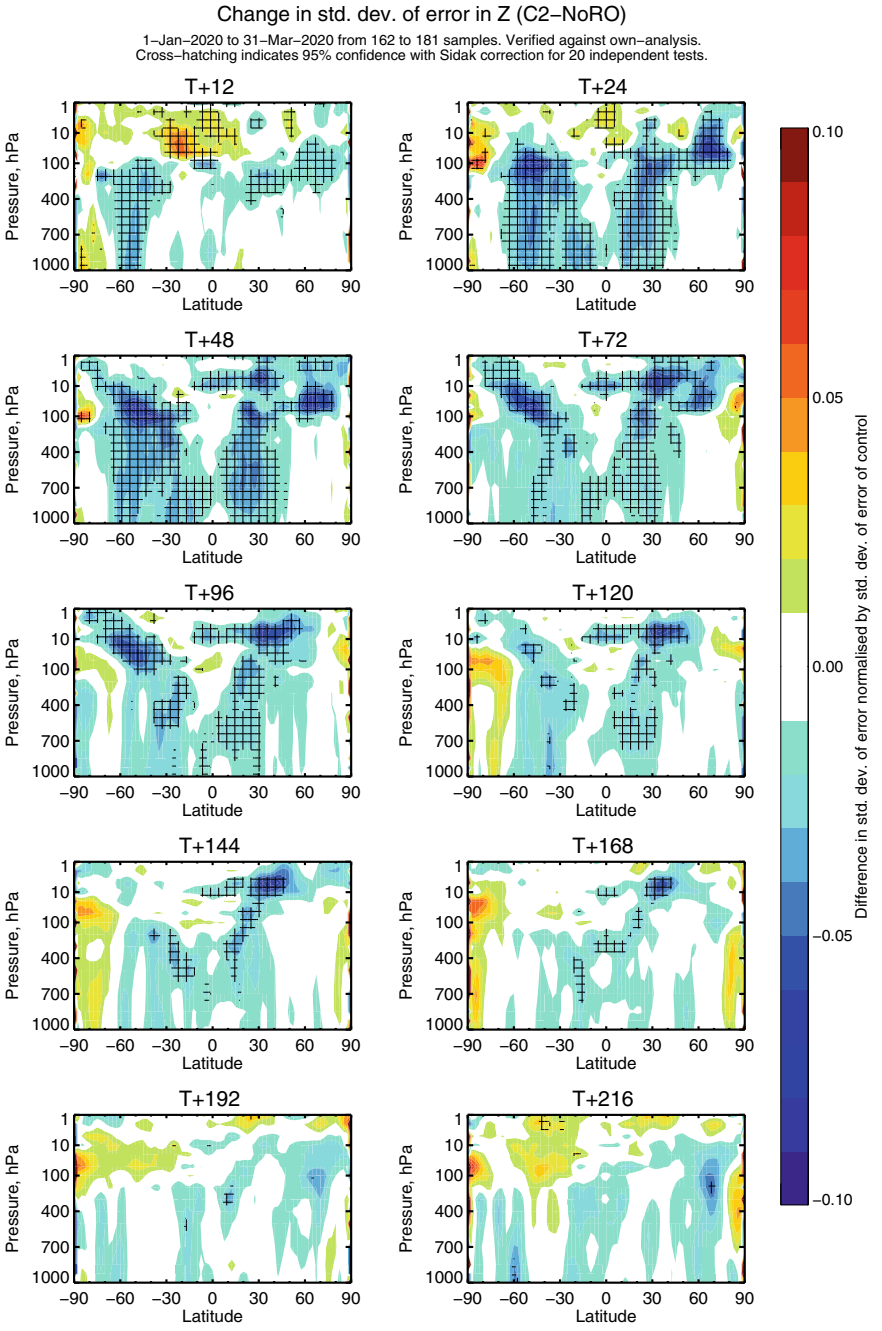

Fig. 9 The zonally averaged fractional change in the standard deviation of the geopotential forecast errors shown as a function of forecast range. The results are comparing the C2 and NoRO experiments, and the verification is against own analysis. The hatching indicates statistical significance at the 95 % level. T+nnn in the figure titles refers to the forecast lead time in hours

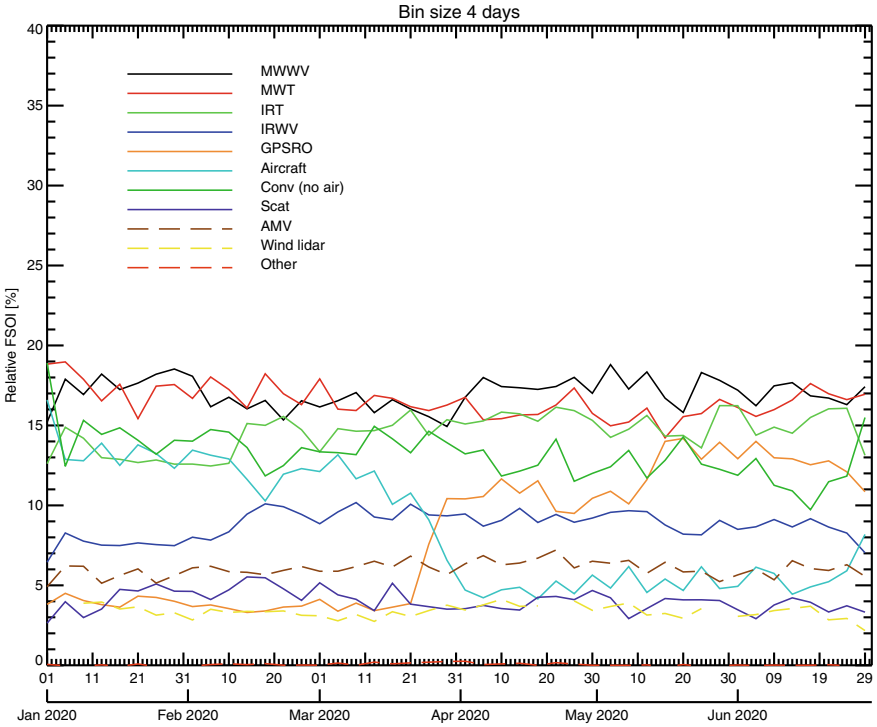

Fig. 10 The timeseries of relative FSOI values for the major observing systems in the ECMWF NWP system. The results are smoothed over 4 d. COSMIC-2 was assimilated from March 25, 2020, and Spire data were used from May 13, 2020

Overall, with the possible exception of 2020, there has been a relatively slow increase in the availability of GNSS-RO measurements since 2006. If some of the concepts described above are adopted routinely, this could increase the density of the observing network. However, an understanding of what constitutes the optimal spatio-temporal sampling is still lacking, and should be devised. An attempt to do just this was done by Harnisch et al. (2013). They examined the reduction in spread of an ensemble of data assimilations when assimilating a number of simulated GNSS-RO observations. They found that the impact did not saturate even when using 128,000 per day. As of 2020, the number of observations routinely available for all operational weather centres is approximately 8000 occultations per day. In the Harnisch et al. (2013) study, it was found that using approxmiately 16 000 profiles accounted for roughly 50% of the benefit of 128 000 occultations, which led the authors to recommend 16,000 - 20,000 occultation profiles per day as a minimum target for future observing networks.

Another new direction being taken in GNSS-RO measurement technique is the use of space-bourne polarametric missions such as the Radio-Occultation and Heavy Precipitation aboard PAZ (ROHP-PAZ) Cardellach et al. (2018). The PAZ spacecraft

has the GNSS payload enhanced to include a dual-polarization RO antenna. The dual-polarization used by the ROHP-PAZ receiver is sensitive to heavy precipitation events and other depolarizing atmospheric effects (e.g. cloud ice). A mission such as this can help to quantify the intense precipitation events, which are known to account for much of the global precipitation totals, but undersampled by the current Earth observing system. Launched on 22 February 2018, the ROHP-PAZ data are being evaluated and disseminated, with standard GNSS-RO profiles being used at many operational weather centers.

Lastly, the enhanced use of the GNSS-RO, whether they are from traditional LEO or LEO-LEO space-based, airborne, and include polarametric information need proper characterization of the uncertainties of the observation themselves. In contrast to radiometers, the degradation of the sensor over time due to changes in the antenna is not present, but stability of the clocks and transmission source of the occulting signal are key parameters which can be used to characterize the differences between the occultations. The satellite systems of the future are likely to be more numerous, but potentially more intermittent and with shorter lifetimes. This will require accurate and voluminous meta-data on the measurements being taken. Having such information can be used for improved analysis and understanding of the different behavoirs and perceived accuracies. To make better use of the GNSS-RO measurements, a more dynamic quality control procedure and observation error assignment could go a long way to delivering the greater potential of these systems.

Acknowledgements This work was supported by funding from the Public Weather Service (PWS) at the Met Office, UK; and by the Office of Naval Reserach. Sean Healy thanks Dr Katrin Lonitz (ECMWF) for help with Sect. 4.

References

Anthes R, Rieckh T (2018) Estimating observation and model error variances using multiple data sets. Atmos Meas Techniq 11:4239–4260. https://doi.org/10.5194/amt-11-4239-2018

Anthes RA, Bernhardt PA, Chen Y, Cucurull L, Dymond KF, Ector D, Healy SB, Ho SP, Hunt DC, Kuo YH, Liu H, Manning K, Mccormick C, Meehan TK, Randel WJ, Rocken C, Schreiner WS, Sokolovskiy SV, Syndergaard S, Thompson DC, Trenberth KE, Wee TK, Yen NL, Zeng Z (2008) The cosmoc/formosat-3—mission early results. Bull Am Meteorol Soc 89(3):313–333. https://doi.org/10.1175/BAMS-89-3-313

Aparicio JM, Deblonde G (2008) Impact of the assimilation of CHAMP refractivity profiles in Environment Canada Global Forecasts. Mon Wea Rev 136:257–275. https://doi.org/10.1175/2007MWR1951.1

Aparicio JM, Laroche S (2011) An evaluation of the expression of the atmospheric refractivity for GPS signals. J Geophys Res 116(D11). https://doi.org/10.1029/2010JD015214

Bean BR, Dutton EJ (1968) Radio meteorology. Dover Publications, New York

Benzon HH, Hoeg P (2016) Wave optics-based leo-leo radio occultation retrieval. Radio Sci 51(6):589–602. https://doi.org/10.1002/2015RS005852

Bowler NE (2020) An assessment of GNSS radio occultation data produced by spire. Q J R Meteorol Soc (2020). https://doi.org/10.1002/qj.3872

Cardellach E, Tomas S, Rius A, Ao CO, de la Torre-Juarez M, Padulles R, Turk FJ, Schreiner B (2018) Polarimetric gnss radio-occultations aboard paz: Commissioning phase and preliminary results. In: IGARSS 2018 - 2018 IEEE International symposium on geoscience and remote sensing IGARSS, pp. 935–937 (2018). 38th IEEE International geoscience and remote sensing symposium (IGARSS), Valencia, SPAIN, 22–27, 2018

Cardinali C (2009) Monitoring the observation impact on the short-range forecast. Q J R Meteorol Soc 135(638):239–250. https://doi.org/10.1002/qj.366

Chen SY, Huang CY, Kuo YH, Guo YR, Sokolovskiy S (2009) Assimilation of gps refractivity from formosat-3/cosmic using a nonlocal operator with wrf 3dvar and its impact on the prediction of a typhoon event. Terrest Atmos Ocean Sci 20(1):133–154. https://doi.org/10.3319/TAO.2007.11.29.01(F3C). 6th FORMOSAT-3/COSMIC Mission Early Results Workshop, Vandenberg, CA, APR 15, 2006

Collard A, Healy S (2003) The combined impact of future space-based atmospheric sounding instruments on numerical weather-prediction analysis fields: A simulation study. Q J R Meteorol Soc 129(593, B):2741–2760 (2003). https://doi.org/10.1256/qj.02.124

Cucurull L (2012) Sensitivity of nwp model skill to the obliquity of the gps radio occultation soundings. Atmos Sci Lett 13(1):55–60. https://doi.org/10.1002/asl.363

Cucurull L, Derber JC, Purser RJ (2013) A bending angle forward operator for global positioning system radio occultation measurements. J Geophys Res-Atmos 118(1):14–28. https://doi.org/10.1029/2012JD017782

Cucurull L, Derber JC, Treadon R, Purser RJ (2007) Assimilation of global positioning system radio occultation observations into ncep's global data assimilation system. Mon Weather Rev 135:3174–3193. https://doi.org/10.1175/MWR3461.1

Culverwell ID, Lewis HW, Offiler D, Marquardt C, Burrows CP (2015) The radio occultation processing package. ROPP Atmos Meas Tech 8:1887–1899. https://doi.org/10.5194/amt-8-1887-2015

Desroziers G, Berre L, Chapnik B, Poli P (2005) Diagnosis of observation, background and analysis-error statistics in observation space. Q J R Meteorol Soc 131(613, C):3385–3396 (2005). https://doi.org/10.1256/qj.05.108. 4th WMO International Symposium on Assimilation of Observations in Meteorology and Oceanography, Prague, CZECH REPUBLIC, APR 18-22, 2005

Eyre J (1994) Assimilation of radio occultation measurements inot a numerical weather prediction system. Technical Report 199, European Centre for Medium-Range Weather Forecasts (1994)

Eyre JR (2016) Observation bias correction schemes in data assimilation systems: a theoretical study of some of their properties. Q J R Meteorol Soc 142:2284–2291. https://doi.org/10.1002/qj.2819

Fjeldbo G, Kliore A, Eshlemen V (1971) Neutral atmosphere of venus as studied with mariner-v radio occultation experiments. Astronom J 76(2):123–124. https://doi.org/10.1086/111096

Gorbunov ME, Lauritsen KB (2004) Analysis of wave fields by Fourier Integral Operators and their application for radio occultations. Radio Sci 39. https://doi.org/10.1029/2003RS002971

Hajj G, Kursinski E, Romans L, Bertiger W, Leroy S (2002) A technical description of atmospheric sounding by gps occultation. J Atmos Solar-Terrest Phys 64(4):451–469. https://doi.org/10.1016/S1364-6826(01)00114-6

Harnisch F, Healy SB, Bauer P, English SJ (2013) Scaling of GNSS radio occultation impact with observation number using an ensemble of data assimilations. Mon Weather Rev 141:4395–4413

Healy S (2001) Radio occultation bending angle and impact parameter errors caused by horizontal refractive index gradients in the troposphere: A simulation study (vol 106, pg 11,875, 2001). J Geophys Res-Atmos 106(D20):24087. https://doi.org/10.1029/2001JD001201

Healy S, Thepaut J (2006) Assimilation experiments with champ gps radio occultation measurements. Q J R Meteorol Soc 132(615, B):605–623. https://doi.org/10.1256/qj.04.182

Healy SB (2014) Implementation of the ropp two-dimensional bending angle observation operator in an nwp system. Technical report 19, EUMETSAT ROM SAF

Healy SB, Eyre JR, Hamrud M, Thepaut JN (2007) Assimilating gps radio occultation measurements with two-dimensional bending angle observation operators. Q J R Meteorol Soc 133(626, A):1213–1227 (2007). https://doi.org/10.1002/qj.63

Hollingsworth A, Lonnberg P (1986) The statistical structure of short-range forecast errors as determined from radiosonde data 1. the wind field. Tellus A - Dyn Meteorol Oceanography 38:111–136

Jensen A, Lohmann M. Benzon HH, Nielsen A (2003) Full spectrum inversion of radio occultation signals. Radio Sci 38:1040. https://doi.org/10.1029/2002RS002763

Jensen A, Lohmann M, Nielsen A, Benzon HH (2004) Geometrical optics phase matching of radio occultation signals. Radio Sci 39. https://doi.org/10.1029/2003RS002899

Kliore A, Cain D, Levy G, Eshleman V, Drake F, Fjeldbo G (1965) Mariner 4 occultation experiment. Astronaut Aeronaut 3(7):72–73

Kravtsov Y, Orlov Y (1990) Radio meteorology. Springer Series on Wave Phenomena. Springer, Berlin Heidelberg

Kursinski E, Hajj G, Bertiger W, Leroy S, Meehan T, Romans L, Schofield J, McCleese D, Melbourne W, Thornton C, Yunck T, Eyre J, Nagatani R (1996) Initial results of radio occultation observations of earth's atmosphere using the global positioning system. Science 271(5252):1107–1110. https://doi.org/10.1126/science.271.5252.1107

Kursinski E, Hajj G, Schofield J, Linfield R, Hardy K (1997) Observing earth's atmosphere with radio occultation measurements using the global positioning system. J Geophys Res Atmos 102(D19):23429–23465. https://doi.org/10.1029/97JD01569

Langland R, Baker N (2004) Estimation of observation impact using the NRL atmospheric variational data assimilation adjoint system. Tellus Ser A-Dyn Meteorol Oceanogr 56(3):189–201. https://doi.org/10.1111/j.1600-0870.2004.00056.x

Leroy S (1997) Measurement of geopotential heights by gps radio occultation. J Geophys Res Atmos 102(D6):6971–6986. https://doi.org/10.1029/96JD03083

Lorenc A (1986) Analysis-methods for numerical weather prediction. Q J R Meteorol Soc 112(474):1177–1194. https://doi.org/10.1002/qj.49711247414

Luntama JP, Kirchengast G, Borsche M, Foelsche U, Steiner A, Healy S, von Engeln A, O'Clerigh E, Marquardt C (2008) Prospects of the eps gras mission for operational atmospheric applications. Bull Am Meteorol Soc 89(12):1863+. https://doi.org/10.1175/2008BAMS2399.1

Melbourne W, Davis E, Duncan C, Hajj G, Hardy K, Kursinski E, Meehan T, Young L (1994) The application of spaceborne gps to atmospheric limb sounding and global change monitoring. Technical Report 94-18, National Aeronautics and Space Administration

NOAA / NESDIS: Commercial Weather Data Pilot (CWDP) Round 2 Summary. https://www.space.commerce.gov/wp-content/uploads/2020-06-cwdp-round-2-summary.pdf (2020)

Poli P, Moll P, Puech D, Rabier F, Healy SB (2009) Quality control, error analysis, and impact assessment of formosat-3/cosmic in numerical weather prediction. Terrest Atmos Ocean Sci 20(1):101–113. https://doi.org/10.3319/TAO.2008.01.21.02(F3C). 6th FORMOSAT-3/COSMIC Mission Early Results Workshop, Vandenberg, CA, APR 15, 2006

Rennie MP (2010) The impact of gps radio occultation assimilation at the met office. Q J R Meteorol Soc 136(646, A):116–131. https://doi.org/10.1002/qj.521

Rocken C, Anthes R, Exner M, Hunt D, Sokolovskiy S, Ware R, Gorbunov M, Schreiner W, Feng D, Herman B, Kuo Y, Zou X (1997) Analysis and validation of gps/met data in the neutral atmosphere. J Geophys Res Atmos 102(D25):29849–29866. https://doi.org/10.1029/97JD02400

Rodgers CD (2000) Inverse methods for atmospheric sounding: theory and practice. Ser Atmos Ocean Planetery Phys. World Scientific (2000). https://doi.org/10.1142/3171

Scherllin-Pirscher B, Steiner AK, Kirchengast G, Kuo YH, Foelsche U (2011) Empirical analysis and modeling of errors of atmospheric profiles from gps radio occultation. Atmos Meas Techniq 4:1875–1890. https://doi.org/10.5194/amt-4-1875-2011

Schreiner WS, Weiss JP, Anthes RA, Braun J, Chu V, Fong J, Hunt D, Kuo YH, Meehan T, Serafino W, Sjoberg J, Sokolovskiy S, Talaat E, Wee TK, Zeng Z (2020) Cosmic-2 radio occultation constellation: First results. Geophys Res Lett 47(4). https://doi.org/10.1029/2019GL086841

Shao H, Zou X, Hajj GA (2009) Test of a non-local excess phase delay operator for gps radio occultation data assimilation. J Appl Remote Sens 3

Sokolovskiy S, Kuo Y, Wang W (2005) Assessing the accuracy of a linearized observation operator for assimilation of radio occultation data: Case simulations with a high-resolution weather model. Mon Weather Rev 133(8)

Solheim F, Vivekanandan J, Ware R, Rocken C (1999) Propagation delays induced in gps signals by dry air, water vapor, hydrometeors, and other particulates. J Geophys Res Atmos 104(D8):9663–9670. https://doi.org/10.1029/1999JD900095

Syndergaard S, Kursinsi E, Herman B, Lane E, Flittnerm D (2005) Refractive index mapping operator for assimilation of occultation data. Mon Weather Rev 133(11):2650

Vorobev V, Krasilnikova T (1994) USSR Phys Atmos Ocean 29

Ware R, Exner M, Feng D, Gorbunov M, Hardy K, Herman B, Kuo Y, Meehan T, Melbourne W, Rocken C, Schreiner W, Sokolovskiy S, Solheim F, Zou X, Anthes R, Businger S, Trenberth K (1996) Gps sounding of the atmosphere from low earth orbit: Preliminary results. Bull Am Meteorol Soc 77(1):19–40. https://doi.org/10.1175/1520-0477(1996)077<0019:GSOTAF>2.0.CO;2

Wee TK, Kuo YH, Lee DK (2010) Development of a curved ray tracing method for modeling of phase paths from gps radio occultation: a two-dimensional study. J Geophys Res Atmos 115. https://doi.org/10.1029/2010JD014419

Wickert J, Reigber C, Beyerle G, Konig R, Marquardt C, Schmidt T, Grunwaldt L, Galas R, Meehan T, Melbourne W, Hocke K (2001) Atmosphere sounding by gps radio occultation: first results from champ. Geophys Res Lett 28(17):3263–3266. https://doi.org/10.1029/2001GL013117

Xie F, Haase JS, Syndergaard S (2008) Profiling the atmosphere using the airborne gps radio occultation technique: a sensitivity study. IEEE Trans Geosci Remote Sens 46(11, 1):3424–3435. https://doi.org/10.1109/TGRS.2008.2004713

Yunck T, Liu C, Ware R (2000) A history of gps sounding. Terrest Atmos Ocean Sci 11(1):1–20. https://doi.org/10.3319/TAO.2000.11.1.1(COSMIC)

Zou X, Liu H, Anthes R (2002) A statistical estimate of errors in the calculation of radio-occultation bending angles caused by a 2d approximation of ray tracing and the assumption of spherical symmetry of the atmosphere. J Atmos Ocean Technol 19(1):51–64. https://doi.org/10.1175/1520-0426

Zou X, Vandenberghe F, Wang B, Gorbunov M, Kuo Y, Sokolovskiy S, Chang J, Sela J, Anthes R (1999) A ray-tracing operator and its adjoint for the use of gps/met refraction angle measurements. J Geophys Res Atmos 104(D18):22301–22318. https://doi.org/10.1029/1999JD900450